

Searching for charged Higgs bosons at $\sim \frac{1}{2}$ -1-TeV e^+e^- colliders

Sachio Komamiya

Stanford Linear Accelerator Center, Stanford University, Stanford, California 94309

(Received 11 April 1988)

Possibilities for charged-Higgs-boson searches at $\sim \frac{1}{2}$ -1-TeV e^+e^- colliders are examined. With an integrated luminosity of $\sim 10^{40}$ cm⁻², it is not difficult to find charged-Higgs-boson pair production if the beam energy is not too close to the charged-Higgs-boson mass. Experimental searches for all the major possible decay modes of charged Higgs bosons, i.e., $H^+ \rightarrow t\bar{b}$, $H^+ \rightarrow c\bar{s}$ (or $c\bar{b}$), $H^+ \rightarrow \tau^+ \nu_\tau$, and $H^+ \rightarrow W^+ H_i^0$, where H_i^0 is one of the neutral Higgs bosons, are surveyed in this paper. Searches for charged Higgs bosons in top-quark decays are also discussed. At e^+e^- colliders the background level is low and well controlled compared to searches at hadron colliders (Superconducting Super Collider or CERN Large Hadron Collider). At hadron colliders, except in some very special cases, it is difficult to find charged Higgs bosons.

I. INTRODUCTION

A. Charged Higgs bosons in two-doublet models

Higgs bosons play an important role in the standard model; they are responsible for generating the masses of all the elementary particles (leptons, quark, and gauge bosons). However, the Higgs-boson sector is the most untested one in the standard model. If Higgs bosons are responsible for breaking the symmetry from $SU(2) \times U(1)$ to $U(1)_{EM}$, it is natural to expect that other Higgs bosons are also involved in breaking other symmetries at the grand-unification scale, etc. Higgs bosons may be something like the "ether" (the medium of light before the advent of the special-relativity theory); i.e., they may not really exist. Even in this case we need experimental effort to perform the equivalent of the "Michelson-Morley experiment." In any case it is extremely important to look for the Higgs bosons or for something like them.

If the Higgs sector is nonminimal, in general, there will be physical-charged-Higgs bosons. The minimal extension of the Higgs sector is to add another $SU(2)$ Higgs doublet:

$$\phi_1 = \begin{pmatrix} \phi_1^+ \\ \phi_1^0 \end{pmatrix}, \quad \phi_2 = \begin{pmatrix} \phi_2^+ \\ \phi_2^0 \end{pmatrix},$$

where ϕ_1^+ , ϕ_1^0 , ϕ_2^+ , and ϕ_2^0 are complex fields. Therefore there are initially eight fields. The vacuum expectation values (VEV's) are

$$\langle \phi_1 \rangle = \begin{pmatrix} 0 \\ v_1/\sqrt{2} \end{pmatrix}, \quad \langle \phi_2 \rangle = \begin{pmatrix} 0 \\ v_2/\sqrt{2} \end{pmatrix}.$$

Assuming CP nonviolation, the relative phase between the two vacuum expectation values is zero. The effective vacuum expectation value for this nonminimal model (v) is derived from the sum in quadrature of the individual VEV's, hence $M_{W^\pm} = gv/2 = g[(v_1^2 + v_2^2)]^{1/2}/2$.

Since the ρ parameter ($\rho = M_W^2/M_Z^2 \cos^2 \theta_W$) is experimentally consistent with unity ($\rho = 1.006 \pm 0.008$) (Ref. 1)

the Higgs multiplets are likely to be $SU(2)$ doublets [also any number of $SU(2)$ singlets are allowed].² At least two Higgs doublets are necessary for most supersymmetric models,³ and models with axion need at least two Higgs doublets to exist.⁴ Also technicolor models need more than two composite Higgs doublets.⁵ For the two- $SU(2)$ -doublet models, there are three physical neutral Higgs bosons (H_1^0, H_2^0, H_3^0) and two charged Higgs bosons (H^+ and H^-). Originally there are four neutral and four charged fields but one neutral field and two charged fields are absorbed to give mass to the Z^0 and to W^\pm by the Higgs mechanism. The mass eigenstates of the physical Higgs bosons can be mixtures of the weak eigenstates. There are two mixing angles for two Higgs doublets since the charged and neutral sector do not mix. One of the mixing angles is related to the ratio of the vacuum expectation values. In general, the physical Higgs bosons in the two-doublet model are given by

$$H^\pm = -\phi_1^\pm \sin b + \phi_2^\pm \cos b,$$

$$H_1^0 = \sqrt{2}[(\text{Re}\phi_1^0 - v_1)\cos a + (\text{Re}\phi_2^0 - v_2)\sin a],$$

$$H_2^0 = \sqrt{2}[-(\text{Re}\phi_1^0 - v_1)\sin a + (\text{Re}\phi_2^0 - v_2)\cos a],$$

$$H_3^0 = \sqrt{2}(-\text{Im}\phi_1^0 \sin b + \text{Im}\phi_2^0 \cos b).$$

The mixing angle b is defined by $\tan b = v_2/v_1$. The other angle a is also an arbitrary parameter. The recipe to obtain the above linear combinations is given elsewhere.⁶

Among the neutral Higgs bosons, H_3^0 is a pseudoscalar and the other two are scalars, if their parities are defined through their couplings with fermions. To be more precise, H_3^0 is a CP -odd state and the other neutrals (H_1^0 and H_2^0) are CP -even states, if CP is conserved.⁷ The interactions of Higgs bosons with fermions can be determined from the fermion mass term in the Lagrangian. The couplings are different from model to model and depend on which Higgs boson is most responsible for which fermion mass. An important constraint on the Higgs-boson couplings is that flavor-changing neutral currents (FCNC's) should not be induced by the neutral Higgs bosons (or at

least that FCNC's should be suppressed to within the experimentally allowed level).⁸ FCNC's from the neutral-Higgs-boson sector are absent if fermions with the same electric and weak charges are allowed to couple only to one of the two Higgs doublets (only to ϕ_1^0 or only to ϕ_2^0).

The charged Higgs bosons are expected to be heavier than the W bosons in the minimal supersymmetric models,⁹ but in general the mass is unknown. The phenomenology of the charged Higgs bosons is less ambiguous than that for the neutral ones since there is only one mixing angle b ($\tan b = v_2/v_1$) for the two-doublet model. The couplings of the charged Higgs boson to fermions are constrained by the absence of the FCNC's. There are two typical models which can avoid the FCNC's which might be induced by the neutral Higgs bosons.¹⁰

(1) All the fermions couple only to one of the Higgs doublets and do not couple to the other one. In this case, the relative ratios of the coupling constants of the charged-Higgs boson to fermions are proportional to the fermion mass.

(2) Fermions with weak isospin $I_3 = \frac{1}{2}$ couple only to one of the Higgs doublets and those with $I_3 = -\frac{1}{2}$ couple only to the other doublet. The relative ratios of the coupling constants depend on both the ratio of the vacuum expectation values and the fermion masses.

Of course, many other choices are possible. In any case, the coupling $H^\pm tb$ is larger than that for $H^\pm cs$ and the coupling for $H^\pm cs$ is larger than for $H^\pm ud$.

B. Present mass limits and searches in the near future

Charged Higgs bosons have been looked for at the SLAC and DESY e^+e^- colliders PEP and PETRA. Most of the region up to ~ 19 GeV is excluded independent of the charged-Higgs-boson decay modes.¹¹⁻¹⁴ Limits below the bottom-quark mass are obtained by the CLEO group¹⁵ using the b -quark decays, $b \rightarrow c + H^\pm$ or $u + H^\pm$.

Recently, the ARGUS Collaboration claimed that they found evidence for $B_d^0 \bar{B}_d^0$ mixing.¹⁶ The measured mixing is large:

$$r_d = \frac{\Gamma(B_d^0 \rightarrow \bar{B}_d^0 \rightarrow X')}{\Gamma(B_d^0 \rightarrow X)} = 0.21 \pm 0.08 .$$

This implies the ratio $x_d = \Delta M_{B^0} / \Gamma(B^0)$ is 0.73 ± 0.18 . Within the standard model, the top-quark mass is constrained to be larger than 50 GeV due to the large r_d for reasonably conservative estimates of the Kobayashi-Maskawa (KM) mixing angles and the QCD corrections. However, $B^0 \bar{B}^0$ mixing can be induced by charged-Higgs-boson exchange in the Glashow-Iliopoulos-Maiani (GIM) diagram,^{17,18} even for a relatively light top quark. Hence the top-quark mass may not necessarily be high, if there is a light-charged-Higgs boson which couples to t and b quarks. Furthermore, if the charged Higgs boson is lighter than the top quark and the top quark decays into $b + H^\pm$, the top mass limit obtained by the UA1 Col-

laboration¹⁹ ($M_t > 44$ GeV) may not be valid, since the number of high- p_t isolated leptons is significantly reduced, compared to the standard top decay mediated by a W boson. Therefore we may still find both the top quark and charged Higgs bosons at the SLAC Linear Collider (SLC) or the CERN e^+e^- collider LEP.

If the charged-Higgs-boson mass cannot be reached by SLC/LEP or even by LEP II, we will look at the hadron colliders [Superconducting Super Collider (SSC) or CERN Large Hadron Collider (LHC)] or at the $\sim\frac{1}{2}$ -1-TeV e^+e^- colliders. At SSC or LHC, the charged Higgs boson is produced by the interaction $b + g \rightarrow t + H^-$ (and the charge-conjugated process) and the cross section is typically $\sim 1-100$ pb (Ref. 20). In general, the charged Higgs boson cannot be produced via WZ fusion processes in any Higgs-doublet model, since the HWZ coupling is forbidden, whereas the standard neutral Higgs boson can be produced via WW or ZZ fusion processes. The most promising decay mode to look for is $H^- \rightarrow \tau \bar{\nu}_\tau$, since the QCD background is not very high. However, the background from the process $b + g \rightarrow t + W^-$ with just the same event signature as the signal and a much higher cross section makes the search seem hopeless.²¹ [The case of charged-Higgs-boson production from heavy-quark decay at the SSC (for example, $g + g \rightarrow t + \bar{t} \rightarrow bH^+ + \bar{b}H^-$) is under study.²²] Considering the higher QCD background, it is not at all clear that the decay mode $H^+ \rightarrow t + \bar{b}$ can be found at SSC/LHC, even if the cross is reasonably large.

On the other hand, at $\sim\frac{1}{2}$ -1-TeV e^+e^- colliders, the background conditions are far better and the events are cleaner since there are no spectator jets. In this paper I will demonstrate that it will not be difficult to find the charged Higgs bosons at such e^+e^- colliders. In general, new particles without color are easier to look for at e^+e^- colliders, if such a machine is built, than at hadron colliders.

II. PHENOMENOLOGY

A. Production cross section

The charged Higgs bosons (H^+H^-) are pair produced in e^+e^- annihilation via virtual γ or Z^0 exchange as shown in Figs. 1(a) and 1(b). The total cross section for the process $e^+e^- \rightarrow \gamma, Z^0 \rightarrow H^+H^-$ is given in Ref. 23:

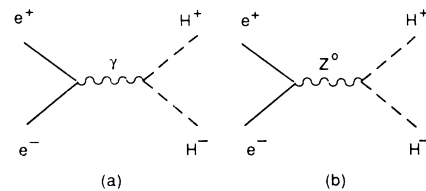


FIG. 1. Feynman diagrams for charged-Higgs-boson pair production in e^+e^- annihilation.

$$\sigma_{H^+H^-} = \frac{1}{4}\sigma_{\mu^+\mu^-}{}_{\text{QED}}\beta^3 \left[1 - 2C_V C_V' \frac{s(s-M_Z^2)}{(s-M_Z^2)^2 + M_Z^2 \Gamma_Z^2} + (C_V^2 + C_A^2)(C_V'^2 + C_A'^2) \frac{s^2}{(s-M_Z^2)^2 + M_Z^2 \Gamma_Z^2} \right],$$

where

$$\beta = \left[1 - \frac{4M_{H^\pm}^2}{s} \right]^{1/2}, \quad C_V = \frac{1 - 4\sin^2\theta_W}{4\sin\theta_W \cos\theta_W},$$

$$C_A = \frac{-1}{4\sin\theta_W \cos\theta_W}, \quad C_V' = \frac{-1 + 2\sin^2\theta_W}{2\sin\theta_W \cos\theta_W}, \quad C_A' = 0.$$

The angular distribution of the H^\pm is $d\sigma/d\Omega \propto \sin^2\theta$.

The cross section relative to that for $q\bar{q}$ plus W^+W^- plus Z^0Z^0 events at the $\sim \frac{1}{2}$ -1-TeV e^+e^- collider is

$$\frac{R_{H^+H^-}}{R_{\text{hadrons}} + R_{W^+W^-} + R_{Z^0Z^0}} \approx \frac{0.3\beta^3}{7+20+1} \approx 0.01\beta^3.$$

The large effects due to radiative corrections and beamstrahlung effects are not taken into account here. After the cut on the polar angle ($|\cos\theta| < 0.6$) the above ratio is about $0.03\beta^3$.

On the Z^0 peak the cross section relative to that for the multihadrons is

$$\frac{\Gamma(Z^0 \rightarrow H^+H^-)}{\sum \Gamma(Z^0 \rightarrow q\bar{q})} = \frac{\Gamma(Z^0 \rightarrow \nu_\mu \bar{\nu}_\mu) \frac{1}{2} \cos^2 2\theta_W \beta^3}{\sum \Gamma(Z^0 \rightarrow q\bar{q})}$$

$$\approx 0.016\beta^3,$$

where the top-quark contribution is neglected. For $|\cos\theta| < 0.6$, the ratio is $0.02\beta^3$. The signal-to-noise ratio is small on the Z^0 peak but the absolute cross section is large.

At PEP/PETRA energies the relative cross section is

$$\frac{R_{H^+H^-}}{R_{\text{hadrons}}} \approx \frac{0.25\beta^3}{4} \approx 0.063\beta^3.$$

For $|\cos\theta| < 0.6$, the ratio is $0.10\beta^3$.

Although the naive estimation of the signal-to-background ratio gives smaller ratios at the high-energy colliders than at PETRA, the background situation is actually better since jet reconstruction is easier at high energies (using electromagnetic and hadronic calorimetry).

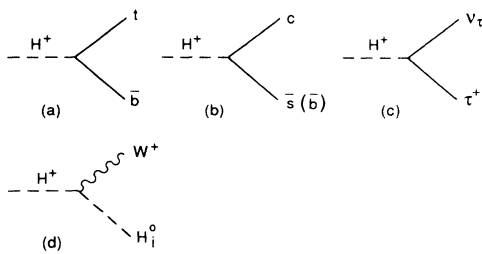


FIG. 2. Feynman diagrams for the charged-Higgs-boson decay processes.

B. Decay of the charged Higgs bosons

The possible decay modes are $H^- \rightarrow b\bar{t}$, $s\bar{c}$ ($b\bar{c}$), or $\tau\bar{\nu}_\tau$ as shown in Figs. 2(a), 2(b), and 2(c). The decay process $H^+ \rightarrow t\bar{b}$ is the dominant mode for most of the parameter space, if it is kinematically allowed. If the mode $H^+ \rightarrow t\bar{b}$ is not allowed, the decay rate to $\tau\bar{\nu}_\tau$ can be significant. For two-doublet models the branching fraction depends on the ratio of the vacuum expectation values. If the ratio of the vacuum expectation values is close to unity, the branching fraction of $H^- \rightarrow \tau\bar{\nu}_\tau$ can be as large as 30%.

The other possibility for the charged-Higgs-boson decay $H^+ \rightarrow H_i^0 + W^+$ [Fig. 2(d)], where H_i^0 is one of the physical neutral Higgs boson, is also considered in this paper. This process is important since the lightest neutral Higgs boson may not be detected at LEP II if the ZZH_i^0 coupling is suppressed. Especially for H_3^0 (CP -odd pseudoscalar state), the ZZH_3^0 and WWH_3^0 couplings are forbidden so that H_3^0 cannot be produced from the process $e^+e^- \rightarrow Z^0H_3^0$ or from WW or ZZ fusion.

Note that the charged Higgs bosons do not couple to $W^+ + Z^0$ at the tree level, if they are members of $SU(2)$ doublets.²⁴ Therefore even if kinematically allowed, the $H^\pm \rightarrow W^+ + Z^0$ decay mode is forbidden (at the tree level).

III. MONTE CARLO STUDIES

For the Monte Carlo studies, a simple detector is assumed, taking into account the energy and angular resolution, and the geometrical acceptance (see Appendix A). Beamstrahlung effects, which are significant at high-energy e^+e^- linear colliders, are also considered (see Appendix B). A typical luminosity distribution as a function of the center-of-mass energy after beamstrahlung is plotted in Fig. 11. All the cross sections are folded with this luminosity function in the analysis.

A. The case for $M_{H^\pm} > M_t + M_b$:

$$e^+e^- \rightarrow H^+H^- \rightarrow t\bar{b} + b\bar{t}$$

The events have approximately a four-jet structure. Reconstruction of the jets and calculation of jet-jet invariant masses are the key points of this analysis. The experimental methods which are described here were mostly developed at PETRA (Ref. 25) and for SLC (Ref. 26). These methods can be applied at the $\sim \frac{1}{2}$ -1-TeV e^+e^- collider, if beamstrahlung effects are not too severe.

Cluster algorithm

To reconstruct the jet structure of the H^+H^- events, a cluster algorithm is introduced. The method is based on the variable d_{ij} (as used in the LUND cluster algorithm),²⁷ which defines the ‘‘distance’’ between two particles (or clusters):

$$d_{ij}^2 = (|\mathbf{p}_i| |\mathbf{p}_j| - \mathbf{p}_i \cdot \mathbf{p}_j)(4|\mathbf{p}_i| |\mathbf{p}_j|) / (|\mathbf{p}_i| + |\mathbf{p}_j|)^2.$$

The variable is a combined measure of the opening angle and momentum imbalance of the two particles (or clusters) i and j . Since there are four jets in the lowest order for the processes $H^+H^- \rightarrow b\bar{t}t\bar{b}$, the number of reconstructed clusters is forced to equal four. The basic scheme goes as follows. Initially, each observed particle is assumed to be a cluster by itself. Then the two clusters with the smallest "distance" d_{ij}^2 are combined by adding vectorially their four-momenta. This is repeated until the number of clusters is reduced to four.²⁶

Event reconstruction

Even with initial-state radiation and beamstrahlung effects, most of the events with large visible energy and with good longitudinal momentum balance can be reconstructed using the beam energy constraint. For any heavy particles which are pair produced, the event shape is little modified by beamstrahlung and initial-state radiation since the events cannot be produced after hard radiation. After finding four clusters (j_1, j_2, j_3, j_4) , the energy of the clusters are calculated assuming that the velocity of the clusters β_i is as observed:²⁵

$$\sum E_i = \sqrt{s}, \quad \sum E_i \beta_i = 0.$$

The calculated energy E_i can be negative for badly reconstructed events.

In the next step, the best combination of two clusters for forming H^+ (or H^-) is searched for. Within the three different combinations, i.e., (12)(34), (13)(24), and (14)(23), the combination with the smallest χ^2 is selected, where

$$\chi^2 = \left[\frac{\sqrt{s}/2 - E_i - E_j}{\sqrt{s}/2} \right]^2 + \alpha \left[\left[\frac{M_{ij} - M_{H^\pm}}{M_{H^\pm}} \right]^2 + \left[\frac{M_{kl} - M_{H^\pm}}{M_{H^\pm}} \right]^2 \right]. \quad (1)$$

The parameter α is optimized so that the reconstructed mass resolution is small for H^+H^- events and, simultaneously, the mass distribution for the background is reasonably wide in order to maximize the signal-to-background ratio. The value $\alpha = 0.25$ is chosen.

Cuts

To enhance the H^+H^- signal relative to ordinary multihadron background, and to WW and ZZ background, the following cuts are applied (the cuts are optimized for 200-GeV H^\pm 's and $\sqrt{s} = 600$ GeV).

(1) $N_{\text{ch}} > 6$, where N_{ch} is the measured charged multiplicity.

(2) $E_{\text{vis}} > 0.7\sqrt{s}$, where E_{vis} is the total visible energy obtained by the electromagnetic and the hadron calorimeter (muon momenta are added).

(3) $|\sum p_z| / E_{\text{vis}} < 0.2$, where $\sum p_z$ is the sum of the longitudinal momenta measured in the same way as the visible energy.

The cuts (2) and (3) reject events with large momentum imbalance along the beam direction due to beamstrahlung and initial-state radiation effects.

(4) $|\cos\theta_{H^\pm}| < 0.70$, where θ_{H^\pm} is the reconstructed polar angle of the H^\pm momentum.

(5) The reconstructed energy of each cluster (E_i , $i = 1, 2, 3, 4$) should exceed 30 GeV.

(6) The difference between the H^\pm and H^\mp energies has to be smaller than 20 GeV.

(7) The difference between the reconstructed " H^\pm mass" and " H^\mp mass" must be smaller than 40 GeV.

(8) The minimum angle (ψ_{min}) between any pair of cluster momenta should be greater than 50° .

The expected ψ_{min} distributions are shown for H^+H^- events assuming $M_{H^\pm} = 150$ GeV in Fig. 3(a), for multihadron events in Fig. 3(b), and for W^+W^- events in Fig. 3(c). After the cuts (1)–(8), the distributions of the averaged invariant mass of the two reconstructed Higgs bosons are shown in Fig. 4(a) for H^+H^- events for $M_{H^\pm} = 150$ GeV. The assumed charged-Higgs-boson mass of 200 GeV is used for the χ^2 calculation in Eq. (1). Hence a small enhancement is seen even above 200 GeV, but this is not a problem for reconstructing the charged-Higgs-boson mass of 150 GeV. In Figs. 4(b), 4(c), 4(d), and 4(e), the same plots are shown for the QCD background, for W^+W^- events, for Z^0Z^0 events, and for the sum of the above three background distributions, respectively. The numbers of events in the figures correspond to an integrated luminosity of 10^{40} cm⁻². It is not difficult to distinguish the charged-Higgs-boson produc-

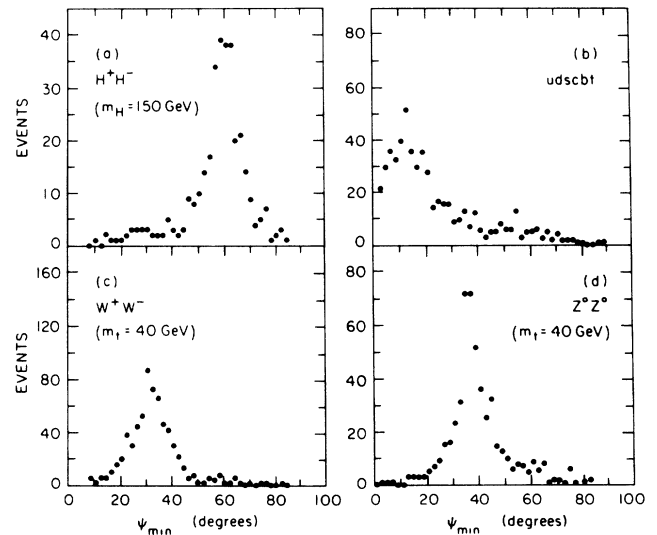


FIG. 3. The distribution of the minimum angle between any pair of the cluster momenta, after the cuts (1)–(7) at $\sqrt{s} = 600$ GeV. (a) For $H^+H^- \rightarrow b\bar{t}t\bar{b}$ events for $M_{H^\pm} = 150$ GeV and $M_l = 60$ GeV, and for an integrated luminosity of $\approx 1.5 \times 10^{40}$ cm⁻². (b) For multihadron events (LUND shower model), for an integrated luminosity of $\approx 0.25 \times 10^{40}$ cm⁻². (c) For W^+W^- events, for an integrated luminosity of $\approx 0.25 \times 10^{40}$ cm⁻². (d) For Z^0Z^0 events, for an integrated luminosity of $\approx 2.0 \times 10^{40}$ cm⁻².

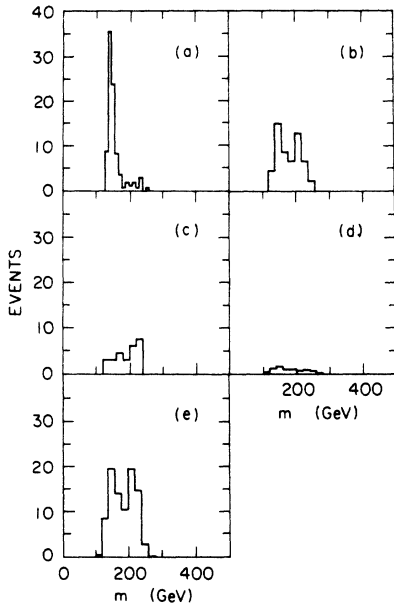


FIG. 4. Invariant-mass (average of the two in an event) distribution of reconstructed charged Higgs bosons for the events passing all the cuts except for the impact parameter cut (9). The cuts are optimized for a 200-GeV charged Higgs boson. Bin size of the plots for the background processes [(b)–(e)] is twice as large as for the signal (a), but the integrated numbers of events are normalized correctly with the luminosity so that the plots can be compared by overlaying the figures. (a) For $H^+H^- \rightarrow b\bar{t}t\bar{b}$ with $M_{H^\pm}=150$ GeV and $M_t=60$ GeV. (b) For multihadron events (LUND shower model). (c) For W^+W^- events. (d) For Z^0Z^0 events. (e) For the sum of (b), (c), and (d). The peaks in the background plot are due to statistical fluctuations because of the small statistics of the Monte Carlo events.

tion from the background. The mass resolution is determined by the jet energy calculation and hence it depends very much on the missing neutrino momenta and energy resolution of the hadron calorimeter (for the details of the resolution, see Appendix A).

Since in an event there are four B hadrons which have a relatively long lifetime of ≈ 1 ps and are heavy (≈ 5

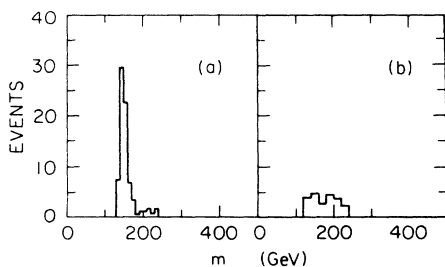


FIG. 5. Invariant-mass distribution of reconstructed charged Higgs bosons for the events after all the cuts (1)–(9). The cuts are optimized for a 200-GeV charged Higgs boson. (a) For $H^+H^- \rightarrow b\bar{t}t\bar{b}$ with $M_{H^\pm}=150$ GeV and $M_t=60$ GeV. (b) For the sum of $q\bar{q}$, W^+W^- , and Z^0Z^0 events.

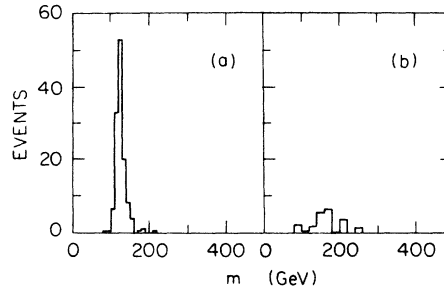


FIG. 6. Invariant-mass distribution of reconstructed charged Higgs bosons at $\sqrt{s}=600$ GeV after applying all the cuts. The cuts are optimized for $M_{H^\pm}=120$ GeV. (a) For the process $H^+H^- \rightarrow b\bar{t}t\bar{b}$ for $M_{H^\pm}=120$ GeV and $M_t=40$ GeV. (b) Corresponding background (sum of QCD, W^+W^- , and Z^0Z^0).

GeV), we can select the events containing charged particles with large impact parameter (distance from the main vertex to the track in the plane perpendicular to the beam) to enhance events with a large number of B hadrons. Assuming an impact parameter resolution of $40 \mu\text{m}$ and a small beam-spot size of $< 1 \mu\text{m}$, the following cut is applied.

(9) At least three charged particles are required to have momentum greater than 1 GeV and have impact parameter between $200 \mu\text{m}$ and 2 mm.

The larger impact-parameter cut of 2 mm reduces the contamination from charged particles coming from K_S or Λ decays. After the cut (9), the reconstructed Higgs-boson mass (average of the two in an event) for 150-GeV H^\pm in Fig. 5(a) and corresponding background processes are shown in Fig. 5(b). Comparing to Fig. 4 shows the background to be largely reduced. In Figs. 6 and 7, the same plots are shown for $M_{H^\pm}=120$ and 200 GeV, respectively. A weaker cut on the minimum angle cut between any pair of clusters ($\psi_{\min} > 40^\circ$) is applied for the case of $M_{H^\pm}=120$ GeV. For $\sqrt{s}=1$ TeV, the mass plot is shown for 300 GeV assuming a top mass of 60 GeV in Fig. 8(a). In Fig. 8(b) the plot is shown for the same Higgs-boson mass but with a top mass of 120 GeV. The

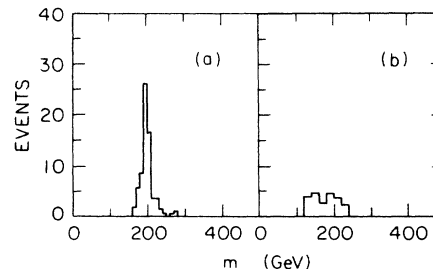


FIG. 7. Invariant-mass distribution of reconstructed charged Higgs bosons at $\sqrt{s}=600$ GeV after applying all the cuts. The cuts are optimized for $M_{H^\pm}=200$ GeV. (a) For the process $H^+H^- \rightarrow b\bar{t}t\bar{b}$ with $M_{H^\pm}=200$ GeV and $M_t=60$ GeV. (b) Corresponding background (sum of QCD, W^+W^- , and Z^0Z^0).

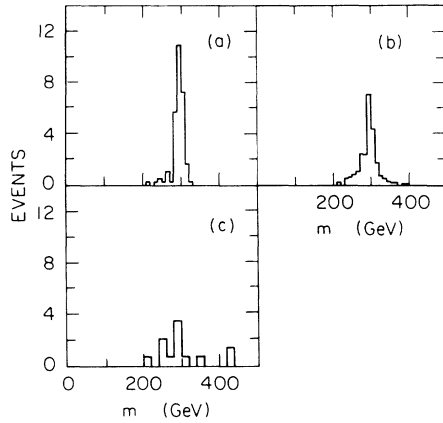


FIG. 8. Invariant-mass distribution of reconstructed charged Higgs bosons at $\sqrt{s}=1$ TeV after applying all the cuts. The cuts are optimized for $M_{H^\pm}=300$ GeV. (a) For the process $H^+H^- \rightarrow b\bar{t}i\bar{b}$ with $M_{H^\pm}=300$ GeV and $M_t=60$ GeV. (b) For the process $H^+H^- \rightarrow b\bar{t}i\bar{b}$ with $M_{H^\pm}=300$ GeV and $M_t=120$ GeV. (c) Corresponding background (sum of QCD, W^+W^- , and Z^0Z^0).

corresponding background plot is shown in Fig. 8(c). Since the top decays into a bottom quark and an on-shell W boson in this case, the events do not have a four-jet structure. The Higgs-boson-mass peak is broader and the efficiency is worse, but the peak is still significant. All the plots are based on the integrated luminosity of 10^{40} cm^{-2} for both $\sqrt{s}=600$ GeV and 1 TeV.

The QCD background is estimated using the LUND QCD shower model (version 6.3) (Ref. 28). We definitely need a parton-shower model in the ~ 1 TeV region, because even at PEP/PETRA energies we often have more than four jets in an event with a reasonable jet resolution. Although the LUND shower model (version 6.3) fits the PEP and PETRA data almost perfectly,²⁹ we are not sure that predictions of this model are reliable in the ~ 1 -TeV region. The model is based on the leading-log approximation (LLA) with the soft and collinear gluon interference effects approximated to by the parton's angular ordering. Because of the leading-log approximation, cross sections for the hard-gluon emission processes are not reliable. For example, the hard three-jet event rate is overestimated, compared to the prediction based on the exact matrix element. (The rate of hard three-jet events is underestimated by the Webber leading-log parton-shower model.³⁰ This difference might depend on the gauge used for the two models.³¹ Although the physical quantities must be gauge invariant at infinite orders of the perturbative calculations, it is not surprising to have different results at lower orders because the models are based on the leading-log approximation.) To obtain the correct parton momentum distribution predicted by the exact $\mathcal{O}(\alpha_s)$ calculations, the first $q\bar{q}g$ branching is modified so that the angular and energy distributions are constrained to be just those given by the $\mathcal{O}(\alpha_s)$ exact calculation. Of course, this modification is not sufficient. If

only a soft gluon is emitted at the first branching and a hard one is emitted at the second branching, then there is no correction for this hard-gluon emission. Therefore, we should not believe that the results of the models are exact. However, even if the QCD background is a factor of 2 larger, this analysis demonstrates that we would still have no problem finding the charged-Higgs-boson signal for the decay scheme $H^+ \rightarrow t + \bar{b}$.

B. $M_{H^\pm} < M_t + M_b$

1. $e^+e^- \rightarrow H^+H^- \rightarrow \tau^+\nu_\tau + s\bar{c}(b\bar{c}), \tau^-\bar{\nu}_\tau + c\bar{s}(c\bar{b})$

If the $H^\pm \rightarrow t + b$ decay is kinematically forbidden, it is worth studying the $\tau\nu$ + hadrons topology since the decay branching fraction for the mode $H^- \rightarrow \tau^-\bar{\nu}_\tau$ can be as large as 30%. The branching fraction depends on the ratio of the vacuum expectation values.

This mode has already been looked for at PETRA and PEP. We can try similar cuts to those applied by JADE at PETRA (Ref. 12) rescaled for $\sqrt{s} \sim 1$ TeV. These cuts are the following.

(1) $N_{\text{ch}} \geq 2$, where N_{ch} is the visible charged multiplicity.

(2) $0.30\sqrt{s} < E_{\text{vis}} < \sqrt{s}$.

(3) $|\cos\theta_{\text{th}}| < 0.7$, where θ_{th} is the polar angle of the thrust axis.

(4) $\phi_{\text{acop}} > 20^\circ$, where ϕ_{acop} is the acoplanarity angle of the event which is defined as follows: The momenta of particles in each hemisphere defined by the thrust axis are summed vectorially. With the two resultant momenta \mathbf{p}_+ and \mathbf{p}_- , the acoplanarity angle ϕ_{acop} is defined as the angle between the plane formed by \mathbf{p}_+ and the beam direction \mathbf{e}_z and the plane formed by \mathbf{p}_- and \mathbf{e}_z :

$$\phi_{\text{acop}} = -(\mathbf{p}_+ \times \mathbf{e}_z) \cdot (\mathbf{p}_- \times \mathbf{e}_z) / |\mathbf{p}_+ \times \mathbf{e}_z| |\mathbf{p}_- \times \mathbf{e}_z| .$$

(5) Each thrust hemisphere is required to have at least one charged particle and an energy of at least 10 GeV. The invariant mass of the four-vector sum in one of the thrust hemispheres M_1 must be larger than 150 GeV and that for the other hemisphere M_2 must be smaller than 5 GeV.

This cut efficiently rejects W^+W^- and Z^0Z^0 events. After all the cuts (1)–(5), the detection efficiency for the H^+H^- events is about 5% for $M_{H^\pm}=200$ GeV and for $B(H^- \rightarrow \tau^-\bar{\nu}_\tau)=0.30$. The number of events expected after all the cuts is about 15, for an integrated luminosity of 10^{40} cm^{-2} , $M_{H^\pm}=200$ GeV, and $B(H^- \rightarrow \tau^-\bar{\nu}_\tau)=0.30$. None of the background events from multihadrons, W^+W^- or Z^0Z^0 events pass the cuts in the Monte Carlo analysis. Because of the limited Monte Carlo statistics of the background events, the 68%-confidence-level (C.L.) upper limit on the number of background events is 2. After selecting the events, the higher one of the two hemisphere masses corrected by the hemisphere visible energy

$$m = M_1(\sqrt{s}/2)/E_1 ,$$

is plotted in Fig. 9, where M_1 is the larger hemisphere mass and E_1 is the corresponding visible energy in the hemisphere. A sharp peak is seen in the plot.

2. Charged Higgs bosons from top-quark decay

We can also look for charged Higgs bosons in top-quark decays, since the decay channel $t \rightarrow H^+ + b$ is fully competitive with the main decay mode $t \rightarrow W^+ + b$. The ratio of the two decay widths is given by²²

$$\frac{\Gamma(t \rightarrow H^+ b)}{\Gamma(t \rightarrow W^+ b)} = \frac{p_{H^+}}{p_{W^+}} \frac{M_t^2(M_t^2 - M_{H^+}^2)}{(M_t^2 + 2M_W^2)(M_t^2 - M_W^2)} \cot^2 b,$$

where p_{H^+} and p_{W^+} are the center-of-mass momenta of the H^+ and W^+ for the respective decays. The cross section of $t\bar{t}$ events is greater than that for charged-Higgs-boson pair production by approximately an order of magnitude:

$$\frac{\sigma(e^+e^- \rightarrow H^+H^-)}{\sigma(e^+e^- \rightarrow \mu^+\mu^-)_{\text{QED}}} \approx 0.3\beta^3 \approx 0.12$$

(for $M_{H^\pm} = 200$ GeV and $\sqrt{s} = 600$ GeV),

$$\frac{\sigma(Z^0 \rightarrow t\bar{t})}{\sigma(e^+e^- \rightarrow \mu^+\mu^-)_{\text{QED}}} \approx 1$$

(for $M_t = 250$ GeV and $\sqrt{s} = 600$ GeV).

Since it is hard to detect the hadronic decay of the charged Higgs boson, the $H^- \rightarrow \tau\bar{\nu}_\tau$ mode is used. The signature of τ 's from the charged-Higgs-boson decay is an isolated charged pion with or without accompanying π^0 's (electromagnetic shower energy). On the other hand, the signature of the ordinary top-quark decay ($t \rightarrow W^+ + b$) is an isolated lepton (e or μ). Of course, isolated charged pions are also produced from the chain $t \rightarrow W^+$

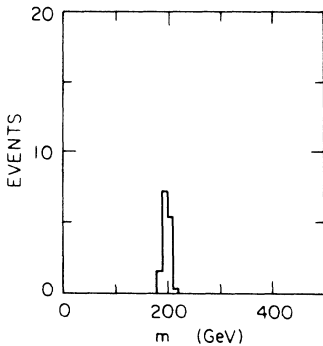


FIG. 9. Plot of the corrected larger hemisphere mass [$m = M_+(\sqrt{s}/2)/E_+$] after all the cuts for H^+H^- events with $M_{H^\pm} = 200$ GeV, and $B(H^+ \rightarrow \tau^+\nu_\tau) = 0.30$, $B(H^+ \rightarrow c\bar{b}) = 0.05$, and $B(H^+ \rightarrow c\bar{s}) = 0.65$ at $\sqrt{s} = 600$ GeV with an integrated luminosity of 10^{40} cm⁻². In the Monte Carlo studies no background events survive after the cuts. Because of the limited statistics for the background calculation, the 68%-C.L. limit of the background events in the plot is set to be 2.

$+b \rightarrow \tau^+\nu_\tau + b \rightarrow \pi^+\bar{\nu}_\tau (+\pi^0s)\nu_\tau + b$. This probability is, however, about a factor of 5 lower than the probability of having an isolated e or μ . Therefore, by comparing the ratio of the number of isolated charged pions over the number of the isolated leptons (e 's or μ 's) to the same ratio expected for ordinary top decays into W^+ alone we can observe, in principle, a signal for the decay $t \rightarrow b + H^+$. [This method was first tried for charged-Higgs-boson searches in $t\bar{t}$ production at SSC (Ref. 22). The background calculation for the QCD processes at SSC is not yet completed.]

The ratio, however, cannot be studied in the absence of the other cuts, since the isolated leptons or isolated charged pions can also come from W^+W^- or Z^0Z^0 events. Therefore, the event topology requirements are also needed to reject the background.

The following set of cuts is proposed.

(1) $E_{\text{vis}} > 0.5\sqrt{s}$.

(2) $|\cos\theta_{\text{th}}| < 0.8$, where θ_{th} is the polar angle of the thrust axis.

(3) Each thrust hemisphere is required to have at least three charged particles. This cut efficiently rejects W^+W^- and Z^0Z^0 events which contain isolated charged particles.

(4) $M_{\text{out}} = (\sqrt{s}/E_{\text{vis}}) \sum p_T^{\text{out}} > 80$ GeV, where p_T^{out} is the transverse momentum of each particle from the plane defined by the two major sphericity axes.³²

In the sample of events obtained by the above cuts, the inclusive numbers of isolated leptons (e 's and μ 's) or isolated charged pions are counted. The isolation condition for the charged particle is as follows.

(5) The momentum must be larger than 2 GeV. The isolation parameter³³ $\rho = [2|\mathbf{p}_i|(1 - \cos\theta_{ji})]^{1/2}$ must satisfy the condition $\rho > 3.0$ GeV^{1/2}, where \mathbf{p}_i is the isolated charged-particle momentum and θ_{ji} is the angle between the isolated charged particle i and the nearest jet J , which is defined by the LUND jet algorithm.²⁷

After the cuts, the numbers of isolated leptons or isolated charged pions are given in Table I. For the first row, $\Gamma(t \rightarrow H^+ + b) = \Gamma(t \rightarrow W^+ + b)$ is assumed. The numbers of events are based on the cross section with initial-state radiation (the maximum initial-state photon energy is 99% of $\sqrt{s}/2$) and with beamstrahlung effects. If the background is taken into account, the ratio (N_{π^\pm}/N_{l^\pm}) for $B(t \rightarrow W^+ b) = 1.0$ (no charged Higgs boson below top mass) is 0.276 ± 0.026 and for the case $B(t \rightarrow H^+ b) = 0.5$ the number is 0.622 ± 0.055 . The above two numbers differ by more than five standard deviations. The ratios are not very sensitive to the top mass as long as the number of isolated π^\pm and l^\pm from the background is small compared with those from the top-quark decays. For a 250-GeV top quark and 150-GeV H^\pm , the effect is still more than four standard deviations if $B(t \rightarrow H^+ b) = 0.5$. Perfect e , μ , and π^\pm identification is assumed here. Since there are not many isolated charged tracks, reasonably conservative values of the $e\mu$ and charged-pion misidentification probabilities do not significantly change the result. For example, with the lepton detection efficiency $P(l \rightarrow l) = 0.9$, the charged-pion efficiency $P(\pi \rightarrow \pi) = 0.9$, the lepton misidentification probability $P(l \rightarrow \pi) = 0.01$, and the pion

TABLE I. Comparison of number of isolated leptons and isolated charged pions. The numbers in the first and the second row are for $t\bar{t}$ events, assuming $\Gamma(t \rightarrow H^+ + b) = \Gamma(t \rightarrow W^+ + b) = 0.5$ and $\Gamma(t \rightarrow W^+ + b) = 1.0$ (no charged-Higgs-boson mode), respectively. The numbers in the table are based on the integrated luminosity of 10^4 pb^{-1} at $\sqrt{s} = 600 \text{ GeV}$ and $M_t = 200 \text{ GeV}$ and $M_{H^\pm} = 150 \text{ GeV}$. The numbers expected for background processes are given in the third to the fifth row, assuming the same luminosity. All the numbers are based on the cross section with initial-state radiation (the maximum initial-state photon energy is 99% of $\sqrt{s}/2$) and with beamstrahlung effects.

Process	Total No. of events	No. of isol. l	No. of isol. π^\pm	N_{π^\pm}/N_{l^\pm}
$t \rightarrow W^\pm$ or $H^\pm + b$	3 436	272	171	0.629 ± 0.061
$t \rightarrow W^\pm + b$ (no H^\pm)	3 436	445	104	0.234 ± 0.025
Light-quark pair ($u\bar{d}sc\bar{b}$)	93 647	4.3	4.0	
W^+W^-	65 100	48	26	
Z^0Z^0	3 858	7.2	5.3	

misidentification probability $P(\pi \rightarrow l) = 0.01$, the ratio N_{π^\pm}/N_{l^\pm} for $B(t \rightarrow W^+ + b) = 1.0$ is 0.286 ± 0.028 , and for the case $B(t \rightarrow H^+ + b) = 0.5$ the number is 0.629 ± 0.058 . The efficiencies and misidentification probabilities are defined within the acceptance of the detector (see Appendix A).

C. Charged-Higgs-bosons decays into $W + H_i^0$:

$$e^+e^- \rightarrow H^+H^- \rightarrow H_i^0W^+ + H_i^0W^- \\ \rightarrow b\bar{b}l^\pm\nu_l + b\bar{b} + q\bar{q}$$

If there is a light neutral Higgs boson, charged Higgs bosons may decay into W plus this light neutral Higgs boson. For the scalar Higgs bosons (CP -even states), the decay branching fraction of the process $H^\pm \rightarrow W^\pm H_i^0$ ($i=1,2$) may be suppressed due to the Higgs-boson mixing. If the lightest Higgs boson is pseudoscalar (CP -odd state H_3^0), there is no such suppression for two-doublet models. This case is more interesting because a pseudoscalar Higgs boson cannot be produced from the process $e^+e^- \rightarrow Z^0H_3^0$ or from WW or ZZ fusion since there is no tree-level ZZH_3^0 or WWH_3^0 coupling. The decay branching fraction of $H^\pm \rightarrow W^\pm H_i^0$ depends on the top mass but it can be the dominant decay mode if H_i^0 is light enough. The dominant decay mode of the H_i^0 is normally $b\bar{b}$. For simplicity, $M_{H^\pm} = 150 \text{ GeV}$, $B(H^\pm \rightarrow W^\pm H_i^0) = 1$, $M_{H_i^0} = 25 \text{ GeV}$, and $B(H_i^0 \rightarrow b\bar{b}) = 1$ are assumed. B -tagging techniques can be used to select these events since each event contains at least four B hadrons.

The most promising process, having a distinctive event topology and the advantage of charged-Higgs-boson mass reconstruction, is when one W decays leptonically and the other W decays hadronically. The events are selected by requiring an isolated lepton from a W decay and also requiring tracks with a large impact parameter (B tagging).

The events are selected by using the same set of cuts for the $t\bar{t}$ selection discussed in the previous section [cuts (1)–(4)]. Also an isolated charged lepton is required. The

isolation condition is just as in the previous section [cut (5)].

Since the event signature is one isolated lepton plus four jets (two H_3^0 jets and two jets from W decay), the selected events are forced to form four clusters using the cluster algorithm discussed in Sec. III A (the isolated lepton is removed from the event for the clustering). The events have to have a W boson, so one of the pairs of jets is required to form the W mass.

(6) A combination of two jets (i and j) exists and satisfies

$$|M_{ij} - M_W| < 5 \text{ GeV}.$$

After all the cuts, the higher hemisphere mass corrected by the hemisphere visible energy $M_1(\sqrt{s}/E_1)$ is plotted in Fig. 10(a). The corresponding background is shown in Fig. 10(b). One can see a clean peak of about 50 events at 150 GeV.

It should be noted that H_3^0 can be found at LEP II if both the H_3^0 and H^\pm are so light that the W^\pm can decay into $H^\pm H_3^0$ (Ref. 34). Since the branching fraction is not large, $\sim 1\%$, the best process to look at is $e^+e^- \rightarrow W^+W^-$ with one W decaying subsequently into

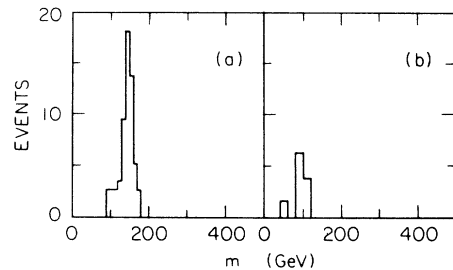


FIG. 10. Plot of the corrected larger hemisphere mass [$m = M_+(\sqrt{s}/2)/E_+$] after all the cuts. (a) For H^+H^- events at $\sqrt{s} = 600 \text{ GeV}$ with integrated luminosity of 10^{40} cm^{-2} , $M_{H^\pm} = 150 \text{ GeV}$, $B(H^+ \rightarrow W^+H_3^0) = 1.00$, $M_{H_3^0} = 25 \text{ GeV}$, and $B(H_3^0 \rightarrow b\bar{b}) = 1.00$. (b) The corresponding background plot for the sum of QCD processes, W^+W^- , and Z^0Z^0 with the same integrated luminosity as for the signal.

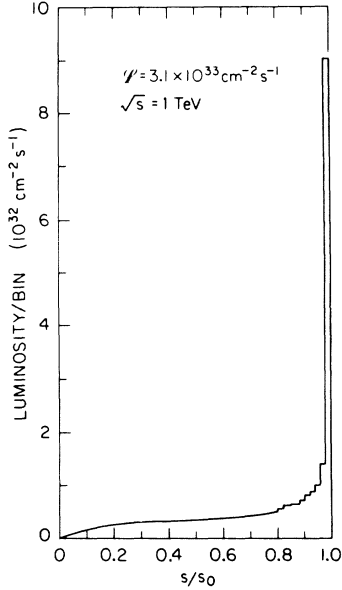


FIG. 11. Plot of the center-of-mass energy squared after the beamstrahlung over the nominal center-of-mass energy squared (s/s_0), where $\sqrt{s_0} = 1$ TeV. The plot is for a typical case with $\bar{\Upsilon} = 0.26$, $E_c/\sqrt{s_0} = 3.3$, and $L = 3.1 \times 10^{33} \text{ cm}^{-2}\text{s}^{-1}$, where $\bar{\Upsilon}$ and E_c are defined in Ref. 32.

$H^\pm H_3^0 \rightarrow \tau^\pm \nu_\tau + b\bar{b}$ and the other W decaying leptonically. Since only the H_3^0 decays hadronically in the event the H_3^0 mass can be reconstructed. Measuring the momentum spectrum of the H_3^0 allows the H^\pm mass to be determined.

IV. CONCLUSIONS

(1) With an e^+e^- linear collider of $\sqrt{s} = \sim \frac{1}{2} - 1$ TeV and an integrated luminosity of $\sim 10^{40} \text{ cm}^{-2}$, we can detect production of charged Higgs bosons and determine its mass for H^\pm masses of less than 80% of the beam energy and a dominant decay mode of $H^+ \rightarrow t + \bar{b}$.

(2) If the charged Higgs boson is sufficiently lighter than the top quark, the top quark decays to $H^+ + b$. We can detect the signal of the charged Higgs boson both through its direct pair production and in the top-quark decay.

(3) If there is a light neutral Higgs boson, a charged Higgs boson may decay into W plus the neutral Higgs boson with a large branching fraction. Even if neutral Higgs bosons cannot be produced via the process $e^+e^- \rightarrow Z^0 H_i^0$, or WW or ZZ fusion (for example, the CP -odd state), the neutral Higgs boson can be produced and detected in the decay $H^\pm \rightarrow W^\pm H_i^0$.

(4) It is necessary to understand the higher-order QCD processes and to improve the QCD shower models, and to test them at lower energies. Also processes containing weak vector bosons must be experimentally understood.

(5) Beamstrahlung effects must be moderate. We have to compromise between the integrated luminosity and the beamstrahlung effect. Beamstrahlung effects as moderate

as we assumed for the Monte Carlo studies (see Fig. 11) are perfectly acceptable for studies of charged-Higgs-boson production.

ACKNOWLEDGMENTS

I would like to thank M. Peskin and G. Feldman who organized the committee for working on physics at $\sim \frac{1}{2} - 1$ -TeV e^+e^- colliders. I appreciate useful discussions with my colleagues in the committee, especially with T. Barklow, P. Burchat, D. Burke, J. Gunion, and H. Haber. I would also like to thank J. Dorfan and P. Rankin for reading and correcting this manuscript. This work was supported by the Department of Energy, Contract No. DE-AC03-76SF00515.

APPENDIX A: MONTE CARLO EVENT SIMULATION

Monte Carlo event generator programs for the process $e^+e^- \rightarrow H^+H^-$ are coded under the framework of the LUND 6.3 generator.²⁸ The production and decay processes are simulated according to the differential cross section and the decay matrix element. For spinless particle pair production, the angular distribution is proportional to $\sin^2\theta$. For the decay, the angular distribution is isotropic in the spinless particle's rest frame. The higher-order QCD effects in the decay processes ($H^- \rightarrow b\bar{t} + g's$) are included by applying the LUND shower model for the decay processes,³⁵ the hadronic fragmentation being simulated by using the LUND string model. Initial-state radiation effects³⁶ and beamstrahlung effects³⁷ are included in the simulation.

The detector effects are not fully simulated, but acceptance cuts, and electromagnetic and hadron energy smearings are applied according to the following parameters.

For stable hadrons (π^\pm , K^\pm , K_L , p , \bar{p} , n , and \bar{n}),

$$\sigma_E/E = 0.50/\sqrt{E} \quad (E \text{ in GeV for } |\cos\theta| < 0.95),$$

$$\sigma_\theta = 5.0 \text{ mrad}, \quad \sigma_\phi = 5.0 \text{ mrad}.$$

For photons and e^\pm 's,

$$\sigma_E/E = 0.15/\sqrt{E} \quad (E \text{ in GeV for } |\cos\theta| < 0.95),$$

$$\sigma_\theta = 3.5 \text{ mrad}, \quad \sigma_\phi = 3.5 \text{ mrad}.$$

For muons

$$\sigma_{p_t}/p_t = 0.001 p_t$$

(p_t is transverse momentum of a muon relative to the beam in GeV, for $|\cos\theta| < 0.85$). The acceptance of each detector component is

$$|\cos\theta| < 0.85 \quad \text{for the tracking chamber}$$

$$|\cos\theta| < 0.95 \quad \text{for the electromagnetic and hadron calorimeter}.$$

It was assumed in the simulation that neutrinos escaped the detector undetected.

APPENDIX B: BEAMSTRAHLUNG

At $\sim \frac{1}{2}$ -1-TeV e^+e^- colliders, there is a significant beamstrahlung effect since the beams must be focused down to a very small size ($< 1 \mu\text{m}$) in order to have a high luminosity of $\sim 10^{33} \text{ cm}^{-2}\text{s}^{-1}$). For these colliders, the particles in one bunch feel the very strong electromagnetic field of the other beam, and the trajectories of individual particles are bent so they emit radiation. Hence, there are two effects: (1) The center-of-mass energy is reduced and the system is boosted along the beam; (2) the electrons and positrons in the beam are often emitted at finite angles to the beam axis. This is called disruption.

Because of the disruption we cannot install detectors in the small polar-angle region. This is why the polar-angle acceptance cut of $|\cos\theta| < 0.95$ is assumed for the calorimeters in this analysis.

A typical luminosity distribution as a function of the center-of-mass energy squared, reduced by the beamstrahlung effect and normalized to the nominal energy squared at 1 TeV², is shown in Fig. 11 (Ref. 37). In the

Monte Carlo analysis, all the cross sections are folded with this luminosity function to correct them.

The reduction of the c.m. energy due to the beamstrahlung effect cannot be distinguished event by event from that due to initial-state radiation where the radiation goes into the beam pipe. The beamstrahlung effect is hard to calculate to a good accuracy using the machine parameters, since these are difficult to measure precisely in real time. Therefore we have to measure experimentally the luminosity as a function of the c.m. energy after beamstrahlung. This luminosity function can be obtained by measuring the numbers of Bhabha events as a function of observed c.m. energy and by unfolding with the theoretical Bhabha cross section after QED radiative corrections. The number of Bhabha events must be measured in the relatively large polar-angle region where the number of electrons or positrons directly due to the disruption are negligible.

To obtain the number of predicted events for any theoretical model this luminosity function must be folded in with the theoretical cross section (with QED radiative corrections).

- ¹G. Altarelli, in *Proceedings of the Twenty-Third International Conference on High-Energy Physics*, Berkeley, 1986, edited by S. Loken (World Scientific, Singapore, 1987), p. 119.
- ²B. W. Lee, in *Proceedings of the XVI International Conference on High-Energy Physics*, Chicago-Batavia, Illinois, 1972, edited by J. D. Jackson and A. Roberts (NAL, Batavia, IL, 1973), Vol. 3, p. 266.
- ³H. E. Haber and G. L. Kane, *Phys. Rep.* **117**, 75 (1984).
- ⁴R. D. Peccei and H. R. Quinn, *Phys. Rev. Lett.* **38**, 1440 (1977); *Phys. Rev. D* **16**, 1791 (1977); W. A. Bardeen and S.-H. H. Tye, *Phys. Lett.* **74B**, 229 (1978); W. A. Bardeen, S.-H. H. Tye, and J. A. M. Vermaseren, *ibid.* **76B**, 580 (1978).
- ⁵S. Dimopoulos and L. Susskind, *Nucl. Phys.* **B155**, 237 (1979); J. Ellis, M. K. Gailard, D. V. Nanopoulos, and P. Sikivie, *ibid.* **B182**, 529 (1981); E. Farhi and L. Susskind, *Phys. Rep.* **74**, 277 (1981).
- ⁶H. E. Haber, G. L. Kane, and T. Sterling, *Nucl. Phys.* **B161**, 493 (1979).
- ⁷J. F. Gunion and H. E. Haber, in *From Colliders to Supercolliders*, proceedings of the Workshop, Madison, Wisconsin, 1987, edited by V. Barger and F. Halzen (World Scientific, Singapore, 1987), p. 67; *Int. J. Mod. Phys.* **A2**, 957 (1987).
- ⁸G. Glashow and S. Weinberg, *Phys. Rev. D* **15**, 1958 (1977).
- ⁹J. F. Gunion and H. E. Haber, *Nucl. Phys.* **B272**, 1 (1986).
- ¹⁰L. F. Abbott, P. Sikivie, and M. B. Weiss, *Phys. Rev. D* **21**, 1393 (1980).
- ¹¹S. Komamiya, in *Proceedings of the 1985 International Conference on Lepton and Photon Interactions at High Energies*, Kyoto, Japan, 1985, edited by M. Konuma and K. Takahashi (Research Institute for Fundamental Physics, Kyoto University, Kyoto, 1986), p. 612.
- ¹²JADE Collaboration, W. Bartel *et al.*, *Phys. Lett.* **114B**, 211 (1982); *Z. Phys. C* **31**, 359 (1986).
- ¹³TASSO Collaboration, M. Althoff *et al.*, *Phys. Lett.* **122B**, 95 (1983).
- ¹⁴CELLO Collaboration, H.-J. Behrend *et al.*, *Phys. Lett. B* **193**, 376 (1987).
- ¹⁵CLEO Collaboration, A. Chen *et al.*, *Phys. Lett.* **122B**, 317 (1983).
- ¹⁶ARGUS Collaboration, H. Albrecht *et al.*, *Phys. Lett. B* **192**, 245 (1987).
- ¹⁷G. G. Athanasiu, P. J. Franzini, and F. J. Gilman, *Phys. Rev. D* **32**, 3010 (1985).
- ¹⁸S. L. Glashow and E. E. Jenkins, *Phys. Lett. B* **196**, 233 (1987).
- ¹⁹UA1 Collaboration, Reports Nos. CERN EP 87-189 and 87-190, 1987 (unpublished).
- ²⁰J. F. Gunion, H. E. Haber, F. E. Paige, W.-K. Tung, and S. S. D. Willenbrock, *Nucl. Phys.* **B294**, 621 (1987).
- ²¹H.-U. Bengtsson, S. Komamiya, and H. Yamamoto, Report No. SLAC-PUB-4368, 1987 (unpublished); in *From Colliders to Supercolliders* (Ref. 7), p. 165; *Int. J. Mod. Phys.* **A2**, 1055 (1987).
- ²²J. F. Gunion, H. E. Haber, S. Komamiya, H. Yamamoto, and A. Barbaro-Galtieri, Reports Nos. SLAC-PUB-4408, SCIPP-87/109, and UCD-87-25, 1987 (unpublished).
- ²³H. Baer *et al.*, in *Physics at LEP*, LEP Jamboree, Geneva, Switzerland, 1985, edited by J. Ellis and R. D. Peccei (CERN Report No. 86-02, Geneva, 1986), p. 297.
- ²⁴J. A. Grifols and A. Mendez, *Phys. Rev. D* **22**, 1725 (1980).
- ²⁵T. L. Barklow, Ph.D. thesis, University of Wisconsin-Madison Report No. RX-1030, 1983.
- ²⁶S. Komamiya, in *Proceedings of the Third Mark II Workshop on SLC Physics*, Pajara Dunes, 1987, edited by G. Feldman (SLAC Report No. 315, Stanford, 1987), p. 253.
- ²⁷T. Sjostrand, *Comput. Phys. Commun.* **27**, 234 (1982); **28**, 229 (1983); **39**, 347 (1986).
- ²⁸T. Sjostrand and M. Bengtsson, *Comput. Phys. Commun.* **43**, 367 (1987).
- ²⁹Mark II Collaboration, A. Petersen *et al.*, *Phys. Rev. D* **37**, 1 (1988).
- ³⁰G. Marchesini and B. R. Webber, *Nucl. Phys.* **B238**, 1 (1984); B. R. Webber, *ibid.* **B238**, 492 (1984).
- ³¹B. R. Webber (private communication).
- ³²R. Marshall, *Z. Phys. C* **26**, 291 (1984).

³³T. L. Barklow, in *Proceedings of the Second Mark II Workshop on SLC Physics*, Granlibakken, 1986, edited by G. Feldman (SLAC Report No. 306, Stanford, 1986), p. 189.

³⁴After essentially completing this paper I found a paper by S. Nandi, *Phys. Lett. B* **202**, 385 (1988).

³⁵A. Petersen modified the decay routine of the LUND model so

that the QCD shower model can be used in the decay of heavy particles.

³⁶F. A. Berends, R. Kleiss, and S. Jadach, *Nucl. Phys.* **B202**, 63 (1982); *Comput. Phys. Commun.* **29**, 185 (1983).

³⁷K. Yokoya, *Nucl. Instrum. Methods* **A251**, 1 (1986); P. Chen, Report No. SLAC-PUB-4293, 1987 (unpublished).